Electronic Supplementary Material (ESI) for Physical Chemistry Chemical Physics.
This journal is © the Owner Societies 2024

Supplementary Information

Physico-geometrical reaction pathway and kinetics of multistep thermal dehydration of calcium chloride dihydrate in a dry nitrogen stream

Kazuki Kato and Nobuyoshi Koga*

Department of Science Education, Division of Educational Sciences, Graduate School of Humanities and Social Sciences, Hiroshima University, 1-1-1 Kagamiyama, Higashi-Hiroshima 739-8524, Japan

Contents

S1. Sample characterization s3

Figure S1. XRD pattern of the sample. s3

Figure S2. FTIR spectrum of the sample. s3

Table S1. Assignment of infrared absorption peaks s3

Figure S3. Particle morphology of the CC-DH sample (300–500 μm) s3

Figure S4. Deliquesce of the CC-DH sample (300–500 μm) observed by standing sample particles at room temperature in an ambient atmosphere: (a) 0, (b) 1, (c) 3, (d) 5, (e) 10, and (f) 15 min. s3

Figure S5. Dehydration of the partially deliquesced CC-DH particle surface observed by standing the sample at 303 K in a stream of dry N_2 (q_v = 100 cm^3 min^{-1}) : (a) 0, (b) 3, (c) 6, and (d) 12 min. s4

S2. Two-step kinetic modeling s4

Weibull function s4

Figure S6. A typical result of MDA for separating the DTG curve for the thermal dehydration of CC-DH to form CC-AH via CC-MH into two DTG peaks using MDA s4

Figure S7. Kinetic curves of each mass loss step of the thermal dehydration of CC-DH to form CC-AH via CC-MH at different β: (a) the first and (b) second mass loss steps. s4

Figure S8. Results of the formal kinetic analysis for each mass loss step separated by MDA: (a) Friedman plots for the first mass loss step, (b) Friedman plots for the second mass loss step, (c) $E_{a,i}$ values at different α_i values, and (d) experimental master plots of ($d\alpha_i/d\theta_i$) versus α_i. s5

Table S2. Kinetic parameters for the first and second mass loss steps determined by MDA to separate into two mass loss steps and formal kinetic analysis of the separated mass loss steps s6

Figure S9. Typical KDA results for the thermal dehydration of CC-DH to form CC-AH assuming an independent two-step process under linear nonisothermal conditions at various β, except for β = 5 K min^{-1} shown in Figure 5(a). s7

Figure S10. Typical KDA results for the thermal dehydration of CC-DH to form CC-AH assuming an independent two-step process under CRTA conditions at various C, except for C = 10 μg min^{-1} shown in Figure 5(b). s8

* Corresponding author. E-mail: nkoga@hiroshima-u.ac.jp

Figure S11. Kinetic curves under linear nonisothermal conditions at different β for each reaction step obtained from the results of KDA based on the two-step kinetic modeling: (a) first and (b) second reaction steps. s9

Figure S12. Kinetic curves under CRTA conditions at different C for each reaction step obtained from the results of KDA based on the two-step kinetic modeling: (a) first and (b) second reaction steps. s9

S3. Three-step kinetic modeling s10

Figure S13. Typical KDA results for the thermal dehydration of CC-DH to form CC-AH assuming an independent three-step process under linear nonisothermal conditions at various β, except for $\beta = 5$ K min^{-1} shown in Figure 8(a). s10

Figure S14. Typical KDA results for the thermal dehydration of CC-DH to form CC-AH assuming an independent three-step process under CRTA conditions at various C, except for $C = 10$ μg min^{-1} shown in Figure 8(b). s11

Figure S15. Typical KDA results for the first two reaction steps of the thermal dehydration of CC-DH to form CC-AH assuming an independent three-step process under isothermal conditions at various T, except for $T = 331$ K shown in Figure 8(c). s12

Figure S16. Kinetic curves for the first reaction steps in the three-step modeling of the thermal dehydration of CC-DH to form CC-AH under different heating program modes: (a) linear nonisothermal, (b) CRTA, and (c) isothermal modes. s13

Figure S17. Kinetic curves for the second reaction steps in the three-step modeling of the thermal dehydration of CC-DH to form CC-AH under different heating program modes: (a) linear nonisothermal, (b) CRTA, and (c) isothermal modes. s13

Figure S18. Friedman plots at various α_i values for the first and second reaction steps in the three-step kinetic modeling: (a) first and (b) second reaction steps. s14

Figure S19. TG–DTG curves for the thermal dehydration of CC-DH ($m_0 = 3.03$ mg) to form CC-AH recorded at a β of 3 K min^{-1} in a stream of wet N_2 ($q_v = 200$ cm^3 min^{-1}) characterized by $p(H_2O) = 4.2$ kPa. Measurements were performed using a humidity-controlled TG system constructed by coupling TG–DTA (TG8122, Rigaku) and a humidity controller (me-40DP-2PHW, Micro Equipment Co.). s14

S1. Sample characterization

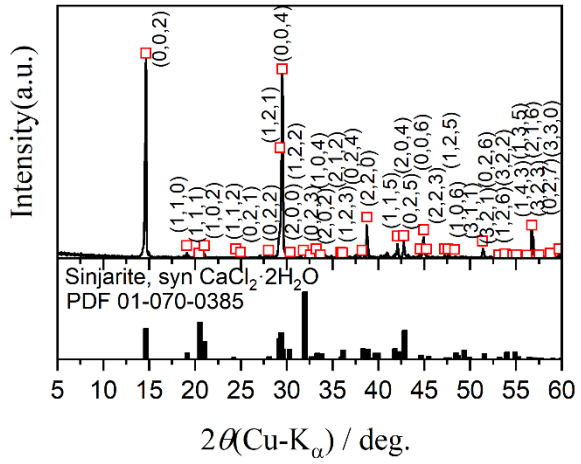

Figure S1. XRD pattern of the sample.

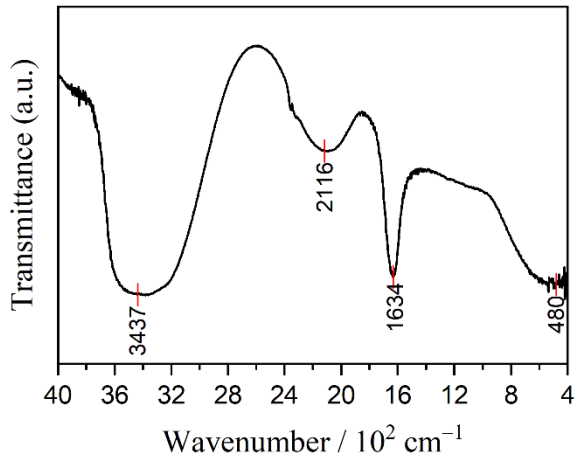

Figure S2. FTIR spectrum of the sample.

Table S1. Assignment of infrared absorption peaks

Wavenumber / cm^{-1}	Vibration mode
3437	O–H stretching band of crystalline water
2116	symmetric O–H stretching vibration
1634	H–O–H bending band of crystalline water
480	Calcium chloride lattice

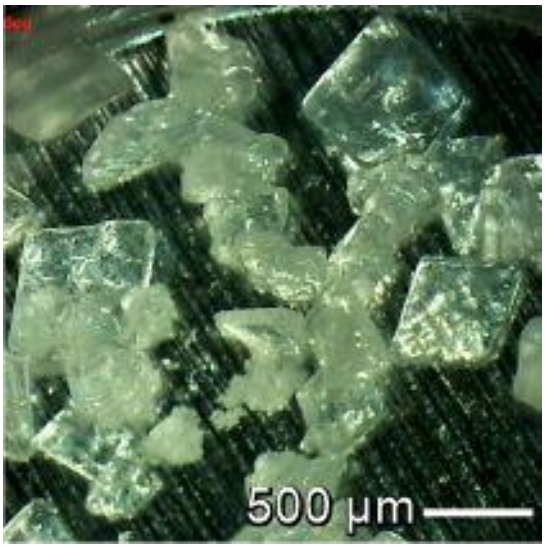

Figure S3. Particle morphology of the CC-DH sample (300–500 µm).

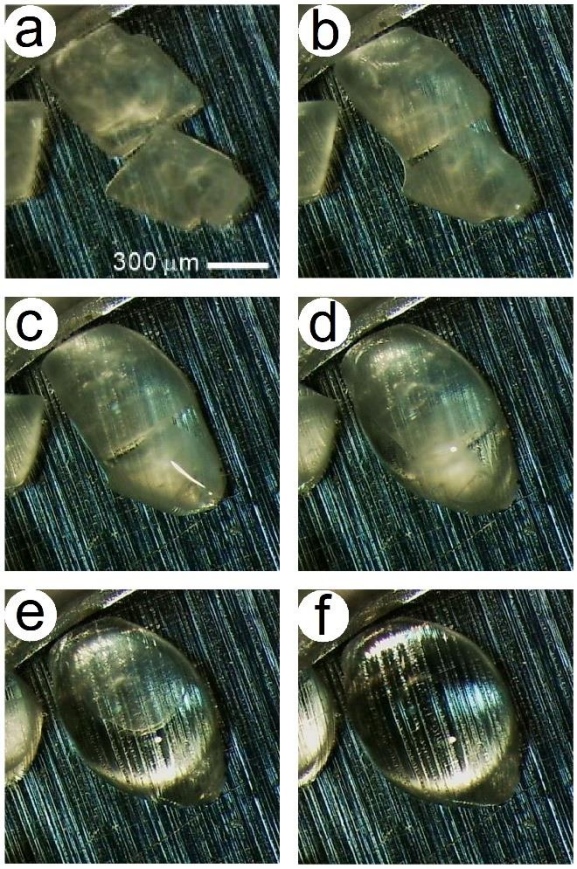

Figure S4. Deliquesce of the CC-DH sample (300–500 µm) observed by standing sample particles at room temperature in an ambient atmosphere: (a) 0, (b) 1, (c) 3, (d) 5, (e) 10, and (f) 15 min.

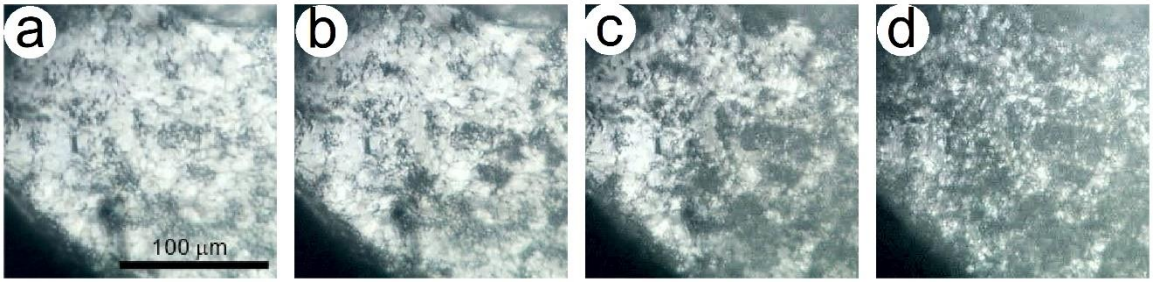

Figure S5. Dehydration of the partially deliquesced CC-DH particle surface observed by standing the sample at 303 K in a stream of dry N_2 (q_v = 100 cm^3 min^{-1}): (a) 0, (b) 3, (c) 6, and (d) 12 min.

S2. Two-step kinetic modeling

Weibull function

$$F(t) = a_0\left(\frac{a_3-1}{a_3}\right)^{\frac{1-a_3}{a_3}}\left\{\frac{t-a_1}{a_2}+\left(\frac{a_3-1}{a_3}\right)^{\frac{1}{a_3}}\right\}^{a_3-1}\exp\left[-\left\{\frac{t-a_1}{a_2}+\left(\frac{a_3-1}{a_3}\right)^{\frac{1}{a_3}}\right\}^{a_3}+\frac{a_3-1}{a_3}\right] \quad \text{(S1)}$$

where a_0 is the amplitude, a_1 is the center, a_2 is the width, and a_3 is the shape parameters.

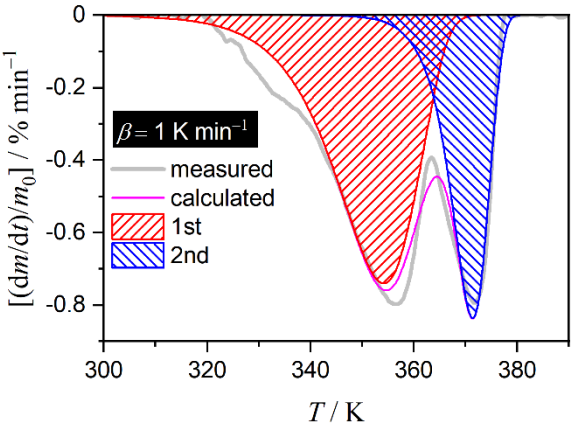

Figure S6. A typical result of MDA for separating the DTG curve for the thermal dehydration of CC-DH to form CC-AH via CC-MH into two DTG peaks using MDA.

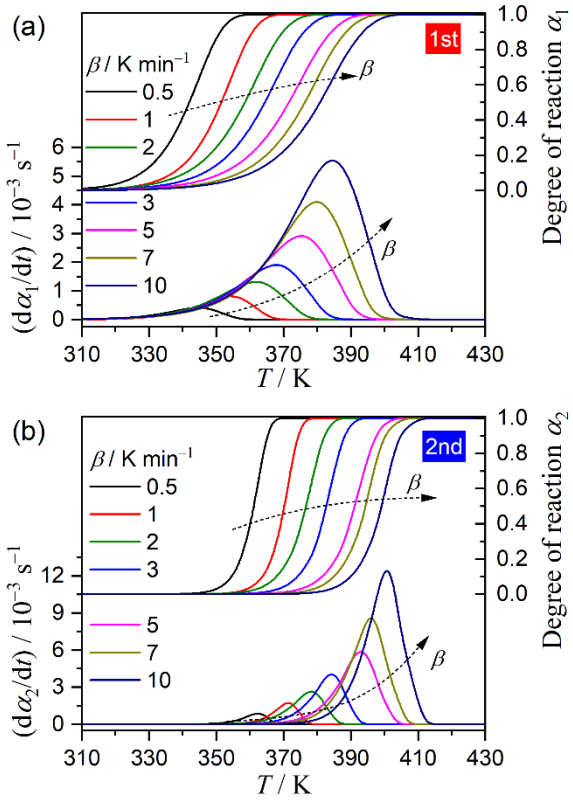

Figure S7. Kinetic curves of each mass loss step of the thermal dehydration of CC-DH to form CC-AH via CC-MH at different β: (a) first and (b) second mass loss steps.

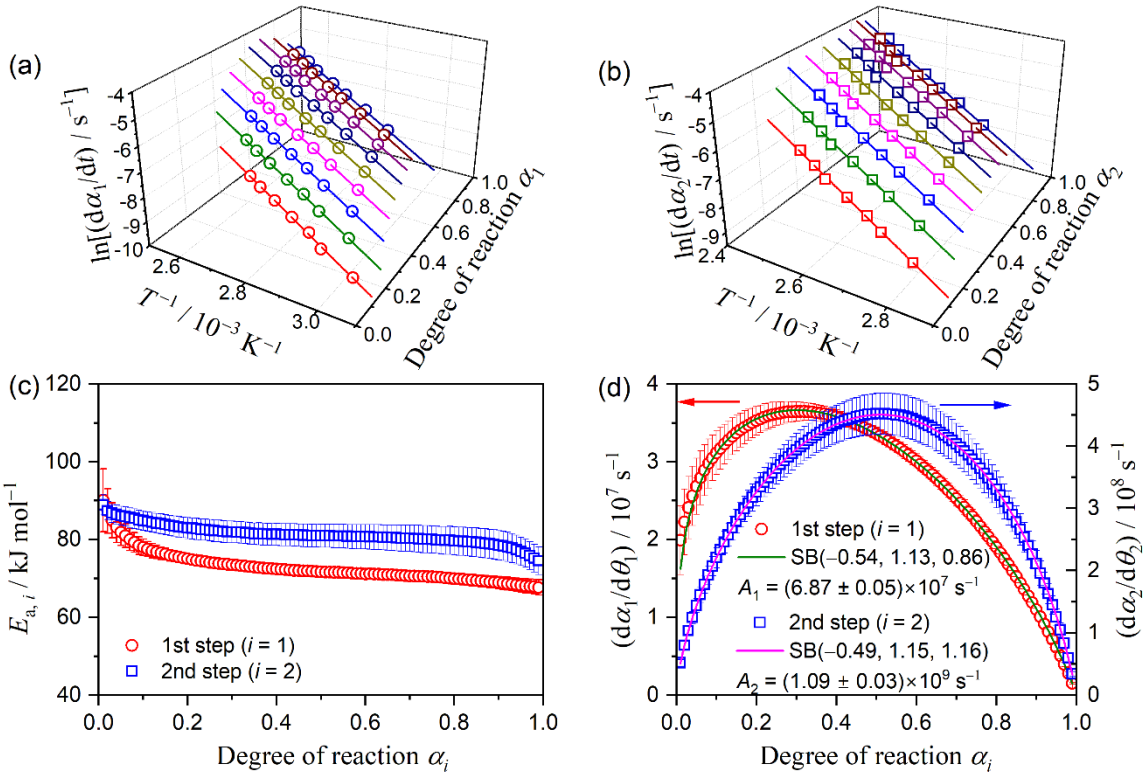

Figure S8. Results of the formal kinetic analysis for each mass loss step separated by MDA: (a) Friedman plots for the first mass loss step, (b) Friedman plots for the second mass loss step, (c) $E_{a,i}$ values at different α_i values, and (d) experimental master plots of $(d\alpha_i/d\theta_i)$ versus α_i.

Table S2. Kinetic parameters for the first and second mass loss steps determined by MDA to separate into two mass loss steps and formal kinetic analysis of the separated mass loss steps

i	c_i	$E_{a,i}$ / kJ mol^{-1}, [a]	$\frac{d\alpha_i}{d\theta_i} = A_i f(\alpha_i)$ with $f(\alpha_i) = \alpha_i^{m_i}(1-\alpha_i)^{n_i}[-\ln(1-\alpha_i)]^{p_i}$				
			A_i / s^{-1}	m_i	n_i	p_i	R^{2}, [b]
1	0.67 ± 0.02	71.6 ± 1.6	(6.87 ± 0.05) × 10^7	−0.54 ± 0.05	1.13 ± 0.02	0.86 ± 0.05	0.9999
2	0.33 ± 0.02	81.2 ± 1.5	(1.09 ± 0.03) × 10^9	−0.49 ± 0.03	1.15 ± 0.01	1.16 ± 0.03	0.9999

[a] Averaged over $0.2 \leq \alpha \leq 0.9$ for $i = 1$ and $0.1 \leq \alpha \leq 0.9$ for $i = 2$.

[b] Determination coefficient of the nonlinear least-squares analysis.

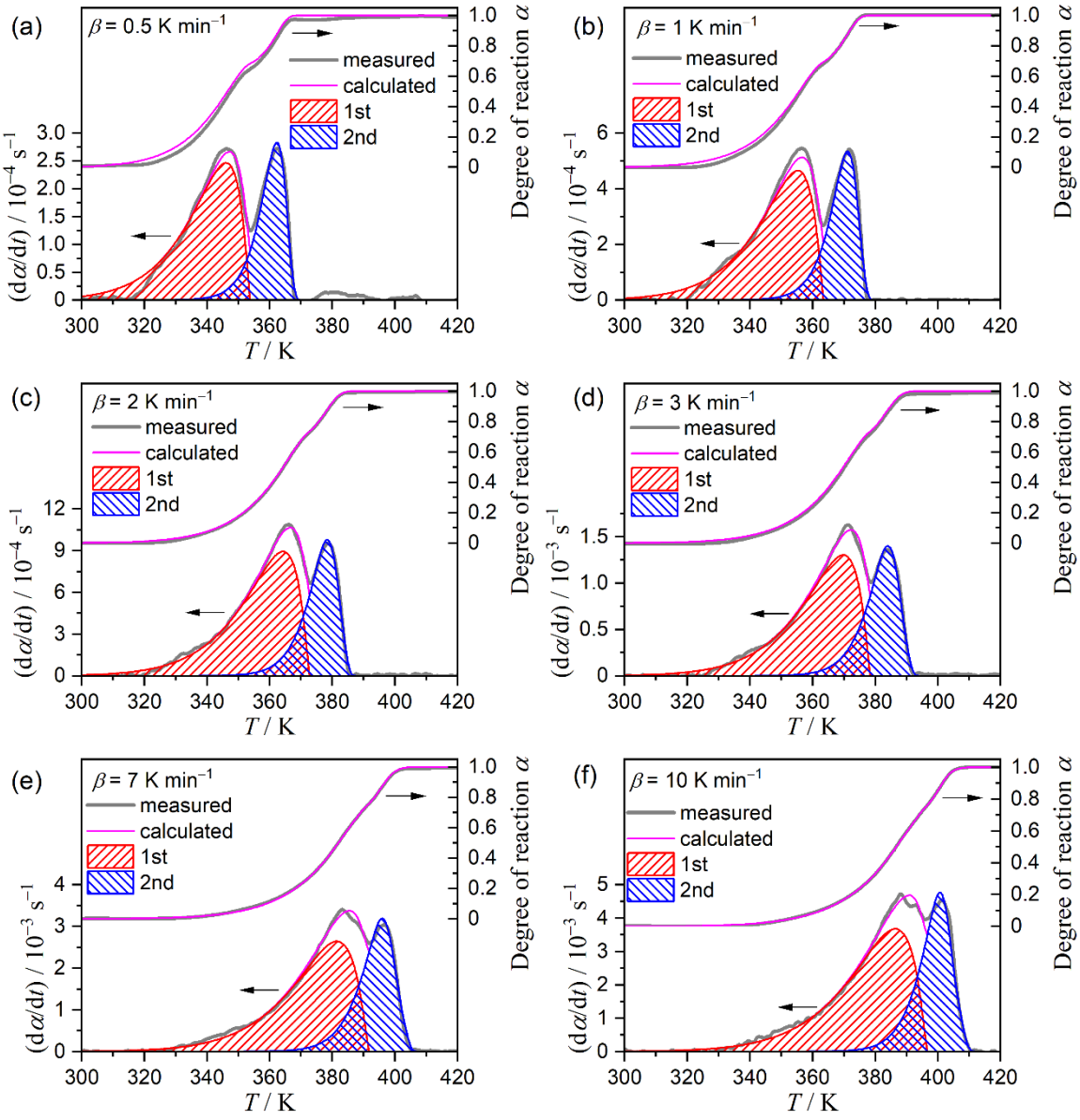

Figure S9. Typical KDA results for the thermal dehydration of CC-DH to form CC-AH assuming an independent two-step process under linear nonisothermal conditions at various β, except for β = 5 K min^{-1} shown in Figure 5(a).

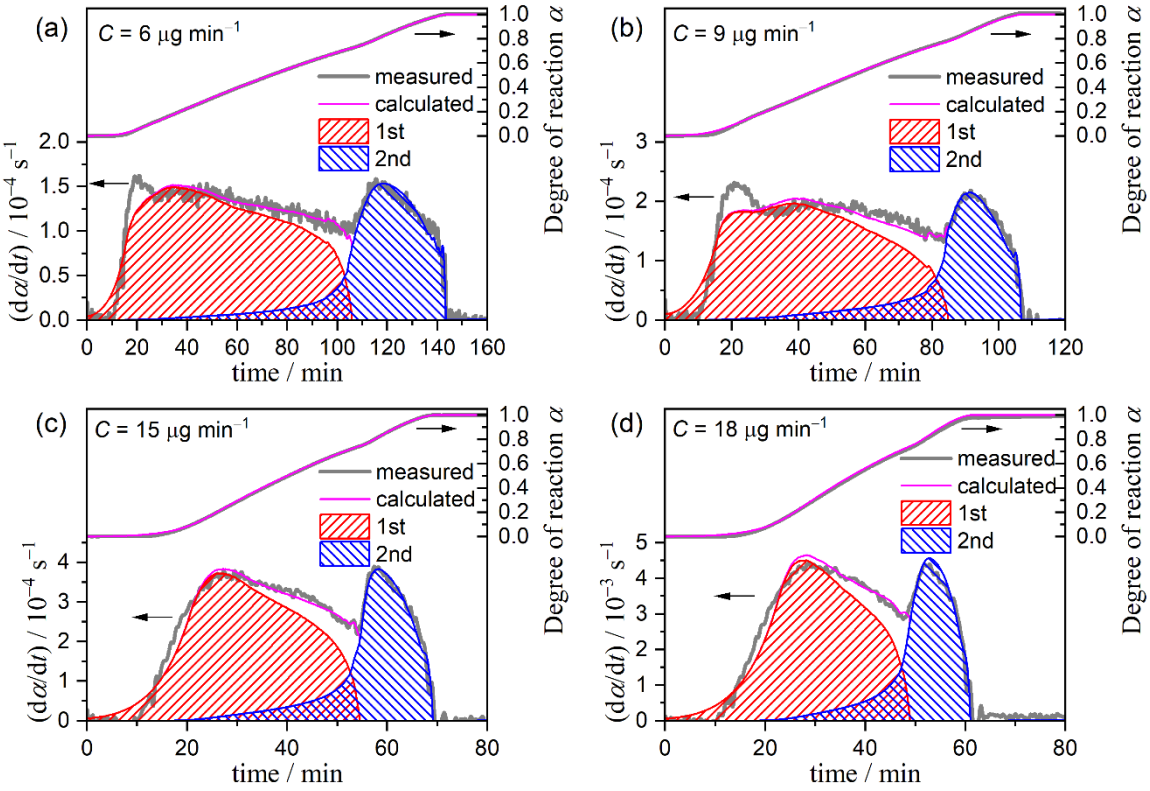

Figure S10. Typical KDA results for the thermal dehydration of CC-DH to form CC-AH assuming an independent two-step process under CRTA conditions at various C, except for C = 12 μg min^{-1} shown in Figure 5(b).

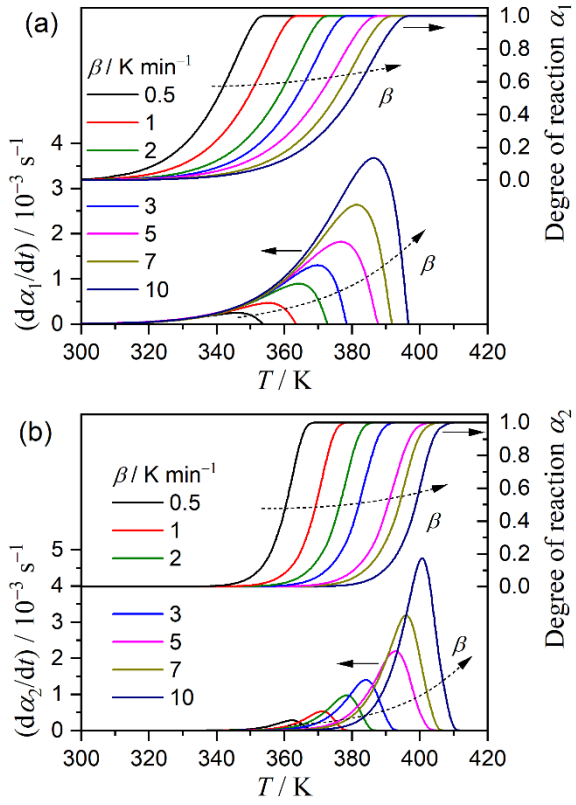

Figure S11. Kinetic curves under linear nonisothermal conditions at different β for each reaction step obtained from the results of KDA based on the two-step kinetic modeling: (a) first and (b) second reaction steps.

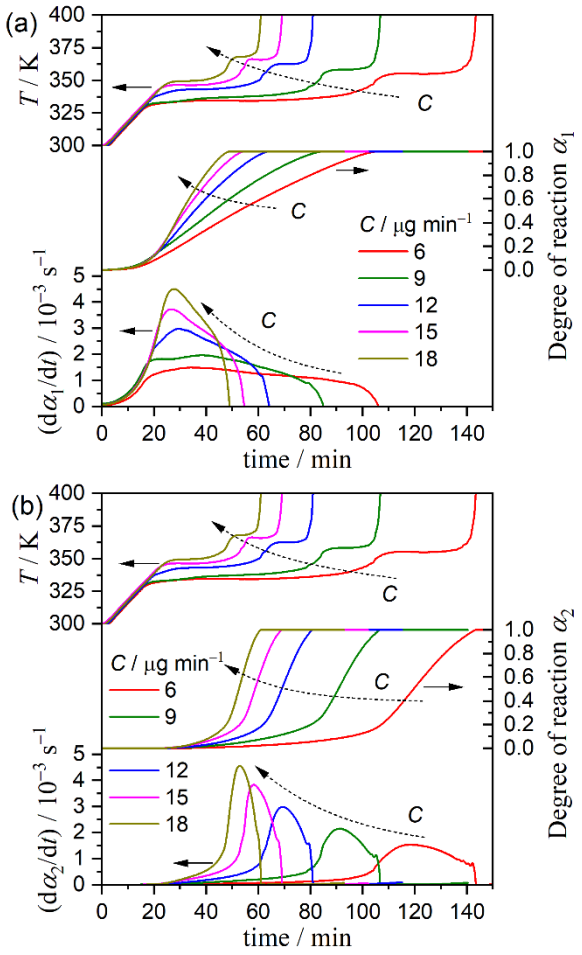

Figure S12. Kinetic curves under CRTA conditions at different C for each reaction step obtained from the results of KDA based on the two-step kinetic modeling: (a) first and (b) second reaction steps.

S3. Three-step kinetic modeling

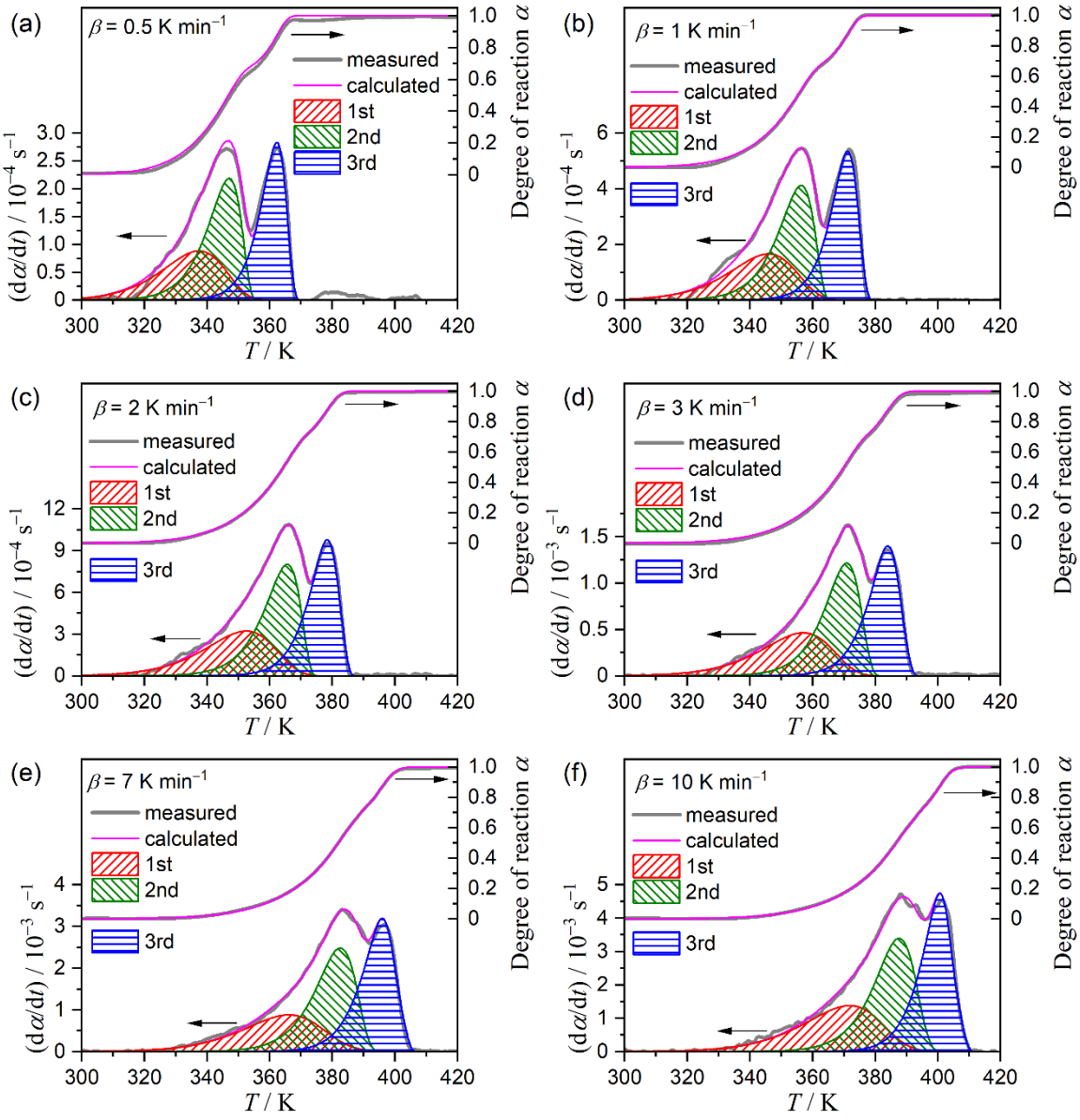

Figure S13. Typical KDA results for the thermal dehydration of CC-DH to form CC-AH assuming an independent three-step process under linear nonisothermal conditions at various β, except for β = 5 K min^{-1} shown in Figure 8(a).

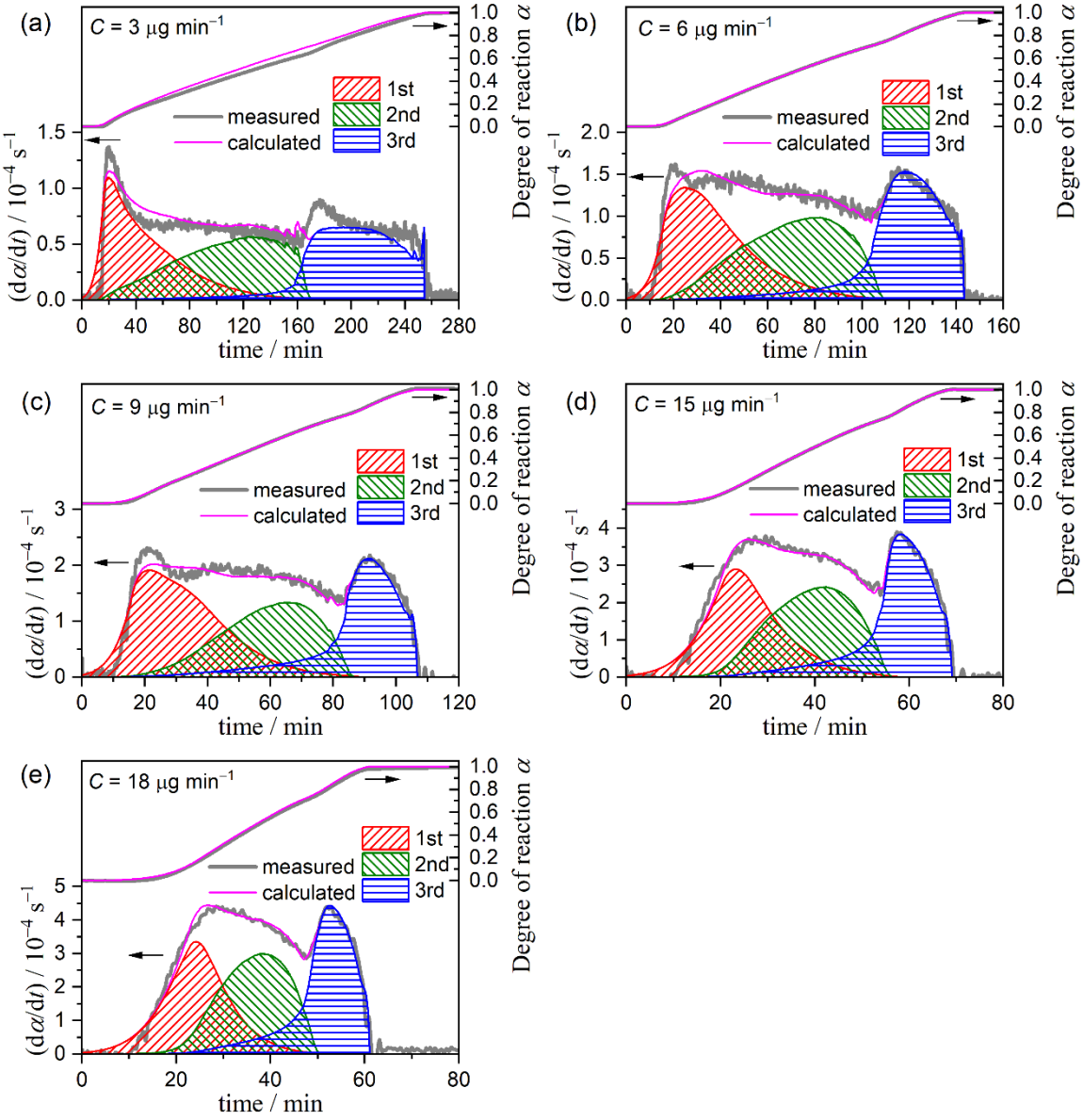

Figure S14. Typical KDA results for the thermal dehydration of CC-DH to form CC-AH assuming an independent three-step process under CRTA conditions at various C, except for C = 12 μg min^{-1} shown in Figure 8(b).

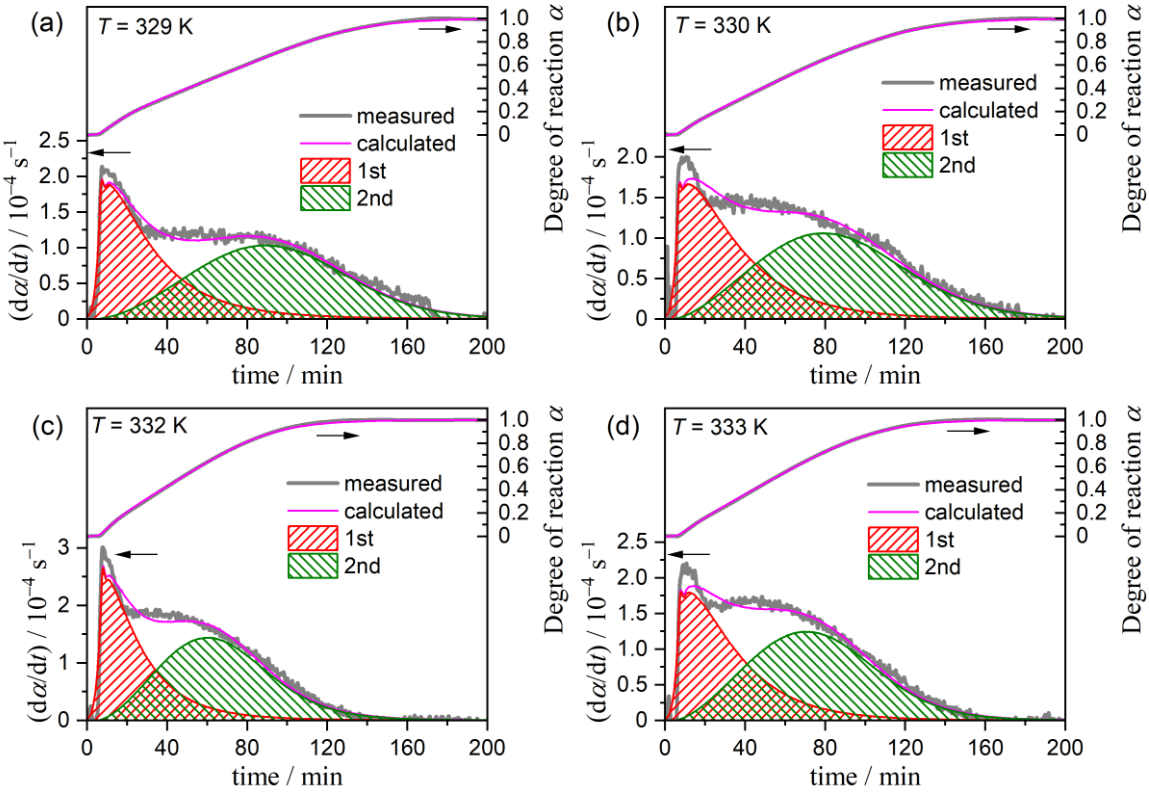

Figure S15. Typical KDA results for the first two reaction steps of the thermal dehydration of CC-DH to form CC-AH assuming an independent three-step process under isothermal conditions at various T, except for T = 331 K shown in Figure 8(c).

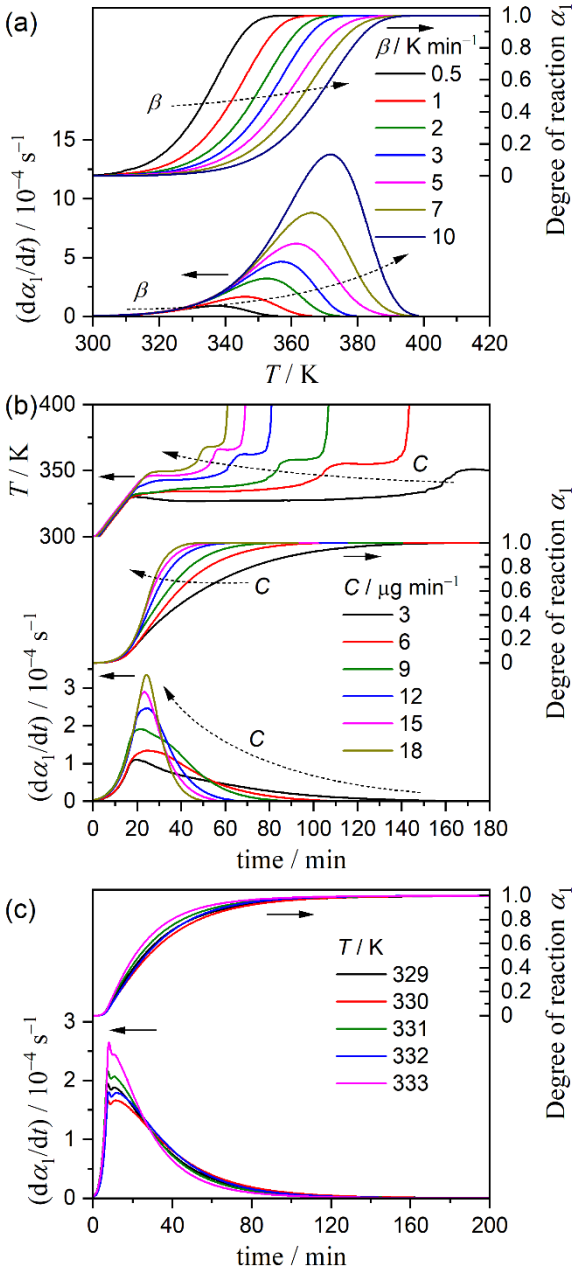

Figure S16. Kinetic curves for the first reaction steps in the three-step modeling of the thermal dehydration of CC-DH to form CC-AH under different heating program modes: (a) linear nonisothermal, (b) CRTA, and (c) isothermal modes.

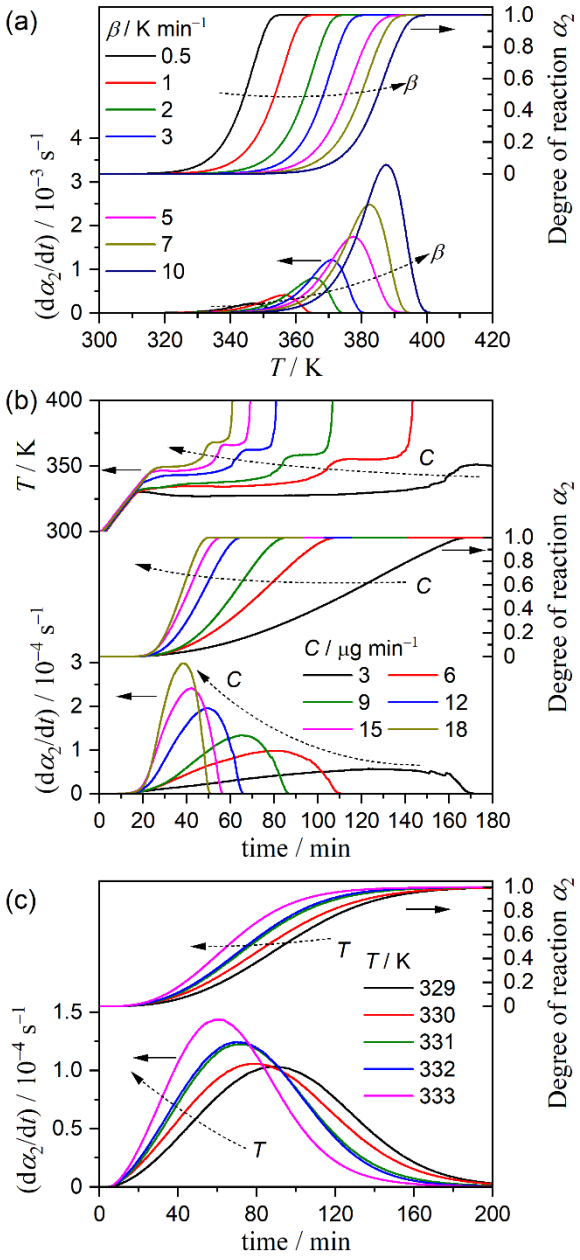

Figure S17. Kinetic curves for the second reaction steps in the three-step modeling of the thermal dehydration of CC-DH to form CC-AH under different heating program modes: (a) linear nonisothermal, (b) CRTA, and (c) isothermal modes.

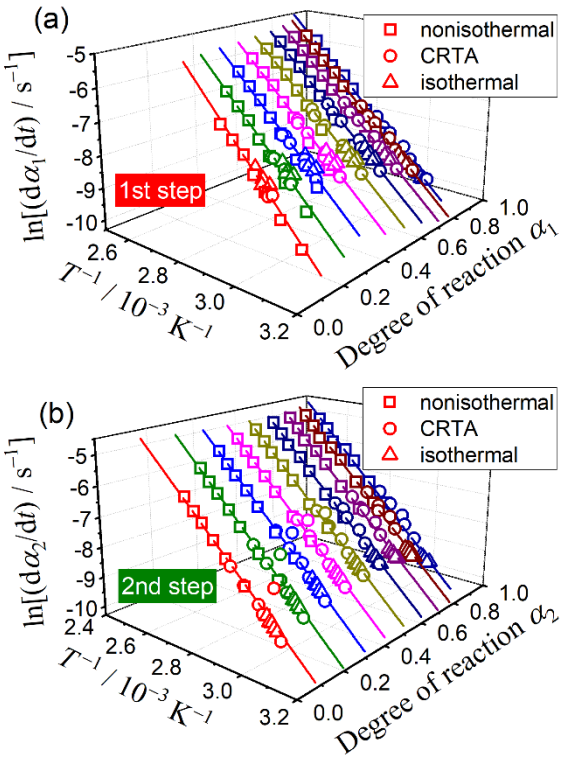

Figure S18. Friedman plots at various α_i values for the first and second reaction steps in the three-step kinetic modeling: (a) first and (b) second reaction steps.

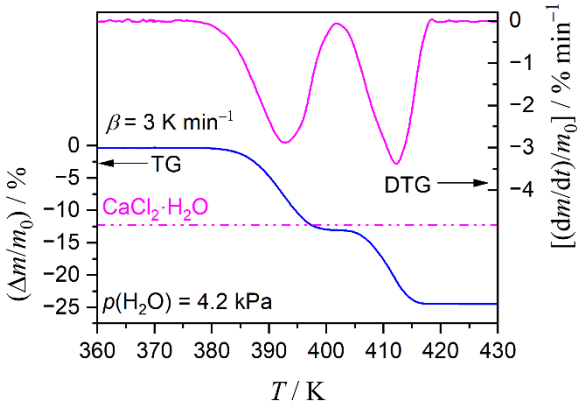

Figure S19. TG–DTG curves for the thermal dehydration of CC-DH (m_0 = 3.03 mg) to form CC-AH recorded at a β of 3 K min^{-1} in a stream of wet N_2 (q_v = 200 cm^3 min^{-1}) characterized by $p(H_2O)$ = 4.2 kPa. Measurements were performed using a humidity-controlled TG system constructed by coupling TG–DTA (TG8122, Rigaku) and a humidity controller (me-40DP-2PHW, Micro Equipment Co.).